In-situ spectroscopic ellipsometry and structural study of HfO_2 thin films deposited by radio frequency magnetron sputtering

Ayten Cantas,[1] Gulnur Aygun,[1,a)] and Deepak Kumar Basa[2]
[1]*Department of Physics, Izmir Institute of Technology (IZTECH), Urla, 35430 Izmir, Turkey*
[2]*Department of Physics, Utkal University, Bhubaneswar 751004, India*

(Received 1 April 2014; accepted 11 August 2014; published online 29 August 2014)

We have investigated the reduction of unwanted interfacial SiO_2 layer at HfO_2/Si interface brought about by the deposition of thin Hf metal buffer layer on Si substrate prior to the deposition of HfO_2 thin films for possible direct contact between HfO_2 thin film and Si substrate, necessary for the future generation devices based on high-κ HfO_2 gate dielectrics. Reactive rf magnetron sputtering system along with the attached *in-situ* spectroscopic ellipsometry (SE) was used to predeposit Hf metal buffer layer as well as to grow HfO_2 thin films and also to undertake the *in-situ* characterization of the high-κ HfO_2 thin films deposited on *n*-type $\langle 100 \rangle$ crystalline silicon substrate. The formation of the unwanted interfacial SiO_2 layer and its reduction due to the predeposited Hf metal buffer layer as well as the depth profiling and also structure of HfO_2 thin films were investigated by *in-situ* SE, Fourier Transform Infrared spectroscopy, and Grazing Incidence X-ray Diffraction. The study demonstrates that the predeposited Hf metal buffer layer has played a crucial role in eliminating the formation of unwanted interfacial layer and that the deposited high-κ HfO_2 thin films are crystalline although they were deposited at room temperature. © *2014 AIP Publishing LLC*.
[http://dx.doi.org/10.1063/1.4893708]

I. INTRODUCTION

The demand for more integrated circuit functionality and performance at lower cost has driven the semiconductor industries to have increased circuit density which, in turn, have resulted in the rapid shrinking of the channel length and gate dielectric thickness of the transistors. This rapid reduction in the dimension of the devices has led to the phenomenal growth of semiconductor industries. However, when the thickness of the silicon dioxide layer, used as the gate dielectric, is less than 1.4 nm, the leakage current due to direct tunneling becomes too large, thus increasing the power dissipation to an unacceptable value and also considerably decreasing the reliability of such thin SiO_2 films against the electrical breakdown.[1–5]

Accordingly, to solve the leakage current problem, films of new materials of physically larger thickness with higher dielectric constant are required to replace such thin SiO_2 films as the gate dielectric. Since silicon nitride ($\kappa = 7$)[6] and silicon oxynitride (in the range between $\kappa = 4$ and $\kappa = 7$)[7] have slightly higher dielectric κ than that of silicon dioxide ($\kappa = 3.9$)[3] and are also compatible with the well established silicon technology, they were studied initially[8] but are less preferred now as gate dielectric, for having too low dielectric constant as compared with high-κ metal oxides.

Although most of the metal oxides offer the possibility as high-κ gate dielectric, thermodynamic stability, i.e., metal oxides must not react with underlying silicon, restricts them to a few metal oxides, such as SrO, CaO, BaO, Al_2O_3, ZrO_2, HfO_2, Y_2O_3, La_2O_3, etc.[3,9–13] The group II oxides like SrO, etc., are not favored as they react with water, the metal oxides, such as Al_2O_3 and Y_2O_3, are not preferred due to their relatively lower dielectric constant, and the oxides like La_2O_3, etc., are not entertained for being more hygroscopic.[13–15] Clearly ZrO_2 and HfO_2 appear promising as high-*k* gate dielectrics but subsequent findings have shown that ZrO_2 is slightly reactive with silicon[9,11,16] and also has higher leakage current compared with HfO_2.[17,18] Because of its high enough κ value, desired energy band offset, and thermodynamic stability with silicon,[3] HfO_2 has emerged as the most promising high-κ gate dielectric ($\kappa = 25$).[9,19] Furthermore, HfO_2 also appears alluring as an important optical material due to its high enough refractive index and broadband transparency.[20,21]

Although the interfacial properties of oxide films play a very crucial role in the performance of the devices, and it is also well known that HfO_2 does not form a perfect interface with silicon, like SiO_2/Si interface, HfO_2 is the most preferred high-κ gate dielectric because of its remarkable properties. Formation of unwanted and unavoidable interfacial SiO_2 layer between HfO_2 and silicon due to the diffusion of oxygen through Si has been reported in the literature.[22–24] In order to prevent the formation of this interfacial layer, some preliminary studies, such as the deposition of Hf metal buffer layer before HfO_2 deposition[23] and also the nitridation of silicon substrate,[22] have been made. Furthermore, in spite of the importance of HfO_2 films as an optical material, very few studies[20,21] and almost no *in-situ* study on the optical properties of HfO_2 have been reported in the literature.

In order to better understand the evolution of optical and interfacial properties of high-κ HfO_2 films, we have undertaken a detailed *in-situ* spectroscopic ellipsometry (SE) and structural studies using Fourier Transform Infrared (FTIR) spectroscopy and Grazing Incidence X-ray Diffraction (GIXRD) of the

a)Author to whom correspondence should be addressed. Electronic mail: gulnuraygun@iyte.edu.tr. Phone: +90 232 750 7715.

HfO_2 films deposited by rf magnetron sputtering on the Hf metal buffer layer predeposited on silicon substrate.

II. EXPERIMENTAL DETAILS

The rf magnetron sputtering setup along with the attached SE used for the deposition as well as *in-situ* and after growth characterization of the studied films is shown in Fig. 1. *n*-type ⟨100⟩ crystalline silicon (c-Si) having resistivity 5–8 ohm cm was used as the substrate. The substrates were cleaned using RCA procedure to remove the organic residues[25] and were then dipped into 1% diluted hydrofluoric (HF) acid for 30 s to remove the native oxides. After these cleaning steps, the substrates were rinsed in de-ionized water and dried with pure N_2 gas before mounting onto the substrate holder. The substrate holder was situated at a distance of 7.4 cm from the target of rf magnetron sputtering system. In order to grow the desired oxide films, the deposition was carried out at room temperature. A 2 in. diameter hafnium metal having 99.9% purity was used as the target material.

In spite of its high purity, Hf target was presputtered for 60 s with argon gas flow to prevent the possible surface contamination of the target. The deposition system was evacuated to a base pressure of about 10^{-6} Torr by a Turbo Molecular Pump (TMP). The working pressure and rf sputtering power were maintained at 2.44×10^{-3} Torr and 42 W, respectively, during the deposition of HfO_2 films at room temperature. Furthermore, to eliminate the formation of unwanted interfacial layer between HfO_2 film and silicon substrate, prior to the deposition of HfO_2 film, a 7 nm thin Hf metal buffer layer was deposited onto the silicon substrate by maintaining the argon flow at 30 sccm (denotes cubic centimeter per minute at STP). After the deposition of Hf metal buffer layer, oxygen gas was introduced at 3 sccm and HfO_2 films were deposited in a mixed oxygen and argon atmosphere maintaining the oxygen to argon flow ratio at 0.1.

While the deposition of thin films continued, simultaneous *in-situ* optical measurements in the 300–850 nm wavelength range of the growing film were carried out with repeated measurements at 20 s time steps by an *in-situ* spectroscopic ellipsometry (Sentech SE801). The spectroscopic ellipsometer attached at a fixed angle of 70° to the deposition chamber is shown in Fig. 1. PSI (Ψ) and DELTA (Δ), the most desired SE parameters of the films, were measured by the phase sensitive detector of rotating analyzer. These SE parameters were modeled and fitted to extract the optical constants *i.e., n* and *k*, thickness, *d*, dielectric constant, ε, transmission coefficient, *T*, and reflection coefficient, *R*, of the studied thin films.

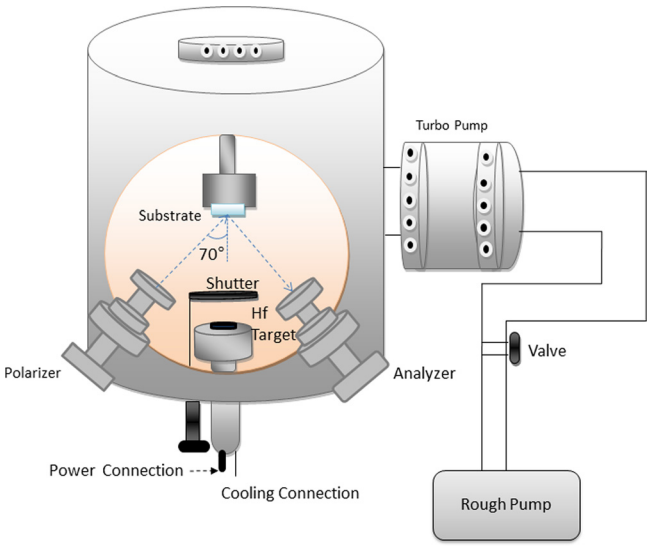

FIG. 1. The schematic representation of a reactive RF sputter growth chamber combined with an *in-situ* spectroscopic ellipsometer.

After the completion of HfO_2 deposition, the grown films were further investigated by FTIR and GIXRD techniques for the structural characterization. IR absorbance measurements between 400 and 1200 cm^{-1} were carried out by a FTIR Bruker Equinox 55 type spectrophotometer having resolution of 0.5 cm^{-1} to study the bonding configurations of the films. The crystalline structure of the films was studied by Panalytical X' Pert Pro MRD type thin film XRD system which was made to operate in grazing incidence mode using 1.5422 A wavelength of CuK_α line having step size and step time of 0.03° and 0.6 s, respectively. The GIXRD patterns were analyzed by X' Pert Highscore software program. The peak matching process was carried out on the observed peak positions by using the specific 2θ values as well as the relative intensity of the peaks.

III. SPECTROSCOPIC ELLIPSOMETRIC MEASUREMENTS OF HfO_2 THIN FILMS

A. Theory of spectroscopic ellipsometry

Spectroscopic ellipsometry for being comprehensive, non-contact, non-destructive, and also offering the possibility of *in-situ* characterization has become an effective surface probe[20,21,26–28] for the optical characterization of thin films of interest. The SE spectra were denoted by the parameters Ψ and Δ. RHO (ρ) represents the amplitude ratio of r_p and r_s, the reflection coefficients of the polarized light corresponding to parallel and perpendicular to the incident plane, respectively, while Ψ denotes the amplitude ratio ($\tan(\Psi) = |r_p|/|r_s|$) and Δ represents the phase shift between *p* and *s* components, respectively. The ellipsometry parameters Ψ and Δ are related to ρ through the relation

$$\rho = \tan\Psi e^{i\Delta} = \frac{r_p}{r_s}. \quad (1)$$

Since spectroscopic ellipsometry is an indirect technique, the desired physical quantities, such as the optical constants, *n* and *k*, and the thickness, *d*, of the films, were derived through a data inversion procedure that requires to build a proper model. The fitting procedure allows to extract the complex dielectric function, ε (hence *n* and *k*), transmission coefficient, *T*, and reflection coefficient, *R*, which are determined through the following equations:

$$\varepsilon = \varepsilon_1 + i\varepsilon_2 = (n+ik)^2 = \sin^2\phi\left[1 + \tan^2\phi\left(\frac{1-\rho}{1+\rho}\right)^2\right], \quad (2)$$

$$R = \frac{(n_2 - n_1)^2 + (k_2 - k_1)^2}{(n_2 + n_1)^2 + (k_2 + k_1)^2}$$
$$T = \frac{n_2}{n_1} \frac{4(n_1^2 + k_1^2)}{(n_1 + n_2)^2 + (k_1 + k_2)^2}, \quad (3)$$

where n, k, ϕ, ε_1, and ε_2 are the refractive index, extinction coefficient, incident angle, real, and imaginary parts of the dielectric constant, respectively.[29] Since the refractive indices $n_1 = 1$ for air, n_2 for the transparent HfO_2 film, and the extinction coefficients $k_1 = 0$ for air, $k_2 = 0$ for transparent HfO_2 film in 300–850 nm spectral range,[30] the above equation (3) reduces to the following equation[28,31,32] as given below:

$$R = \frac{(n_2 - 1)^2}{(n_2 + 1)^2} \quad T = \frac{4n_2}{(1 + n_2)^2}. \quad (4)$$

B. Cauchy model for spectroscopic ellipsometry of HfO_2 layer

The optical model to fit SE data is composed of three layers on the substrate, i.e., Air/HfO_2/SiO_2/c-Si⟨100⟩ which is shown in Fig. 2. The optical constants of HfO_2 film were simulated from Cauchy model. The Cauchy model is a polynomial function[33] which is widely used for dielectrics and semiconductors in spectral regions where they are transparent.[28,30,33–35] It is well known[28] that Cauchy model is an approximate function of Sellmeier model which, in turn, corresponds to a region where $\varepsilon_2 \sim 0$ in the Lorentz model. The equations for the Cauchy model[36] are

$$n(\lambda) = A_0 + \frac{A_1}{\lambda^2} + \frac{A_2}{\lambda^4} + \cdots, \quad (5)$$
$$k(\lambda) = 0, \quad (6)$$

where n, k, λ are refractive index, extinction coefficient, and wavelength, respectively. The wavelength, λ, is in nanometers, and A_0, A_1, and A_2 are numbers to be fitted with respect to wavelength.

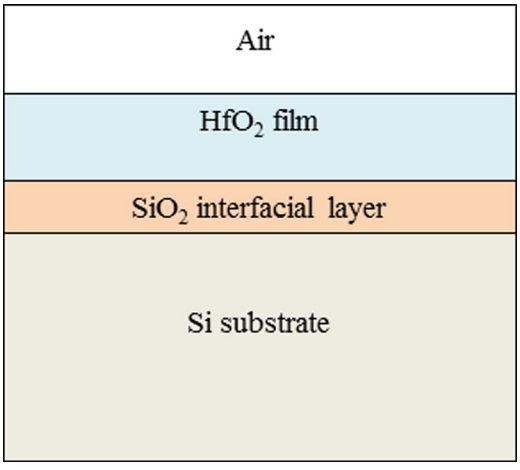

FIG. 2. Film stack used in the modeling and fitting steps of spectroscopic ellipsometer measurements.

C. Data analysis of spectroscopic ellipsometry

Incidence angle of light used for the measurements was 70°, for the measured spectral range of 300–850 nm. Since HfO_2 is transparent in the spectral range of interest, Cauchy dispersion relation has been used as the model to obtain the optical functions of the studied films in the measured spectral region. The use of Cauchy model to study HfO_2 films has also been reported in the literature.[30,37]

The optical constants of the crystalline silicon (Si) substrate and the silicon dioxide (SiO_2), i.e., $n = 1.46$ for stoichiometric SiO_2 were obtained from the literature.[38,39] The parameters, such as thickness and optical constants (n and k) of HfO_2 thin film, were left as variables. Furthermore, since the formation of SiO_2 layer, which depends on the deposition conditions of the studied films, is likely between HfO_2 and Si substrate, thickness of the SiO_2 over layer was also considered as variable.

The dielectric function of the studied films was derived through data analysis using the said optical model. To get the best estimate, the generated Ψ and Δ are fitted to the corresponding experimental data by varying the model parameters. The best fits are achieved by minimizing the mean square error (MSE). The MSE function defines the quality of fit and is given by Eq. (7). MSE determines the curve difference between measured and fitted SE data and the lowest value of it is desired to be obtained in terms of perfect accuracy between measured and fitted data[29,40]

$$MSE = \frac{1}{2N - M} \times \sum_{i=1}^{N} \left[\left(\frac{\psi_i^{\mathrm{mod}} - \psi_i^{\mathrm{exp}}}{\sigma_{\psi,i}^{\mathrm{exp}}} \right)^2 + \left(\frac{\Delta_i^{\mathrm{mod}} - \Delta_i^{\mathrm{exp}}}{\sigma_{\Delta,i}^{\mathrm{exp}}} \right)^2 \right], \quad (7)$$

where N is the total number of data points taken, σ is experimental error, and M is the number of fitted parameters.

IV. RESULTS AND DISCUSSION

A. Spectroscopic ellipsometry study

Figure 3 displays the measured Ψ of the HfO_2 film deposited at time steps of 20, 60, 100, 160, 220, and 280 s. Measured and fitted curves corresponding to the time step of 220 s are shown in the inset of Fig. 3 as a representative example. Similarly, the measured Δ of HfO_2 film deposited at time steps of 20, 60, 100, 160, 220 and 280 s is shown in Fig. 4, while the measured and the fitted curves pertaining to the time step of 220 s are displayed as a representative example in the inset of Fig. 4. The MSE values both for Ψ and Δ are found to be small which is about 1.42. This seems to imply good quality of fit for Ψ as well as for Δ of the studied films.

Figure 5 exhibits the thickness evolution of the growing HfO_2 film as a function of deposition time, and the thickness variation of SiO_2 with deposition time is shown in the inset of Fig. 5. Since the possible natural oxide (SiO_2) formation on silicon substrate is likely when exposed to air, the very

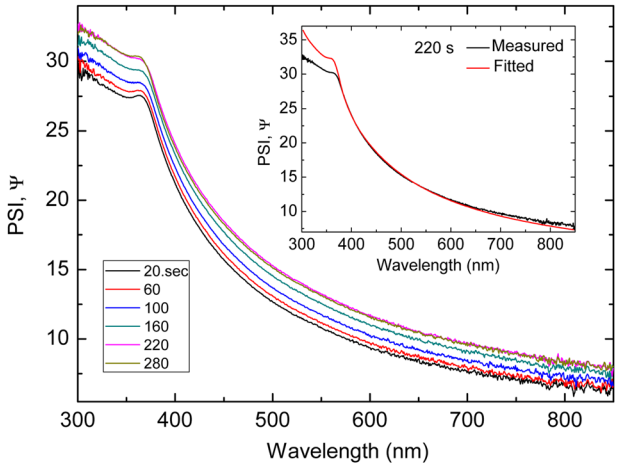

FIG. 3. Ellipsometric measured PSI (Ψ) spectra of the thin HfO_2 layer deposited at the time steps of 20, 60, 100, 160, 220, and 280 s, while inset plot shows the measured and fitted curves corresponding to the time step of 220 s.

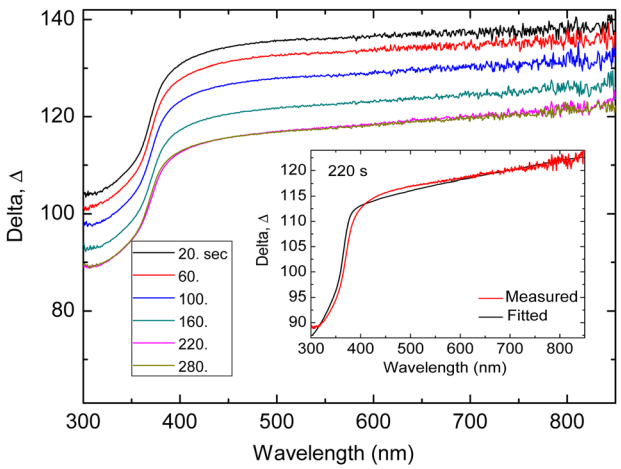

FIG. 4. Ellipsometric measured DELTA (Δ) spectra of the thin HfO_2 layer deposited at the time steps of 20, 60, 100, 160, 220, and 280 s, while inset plot shows the measured and fitted curves pertaining to the time step of 220 s.

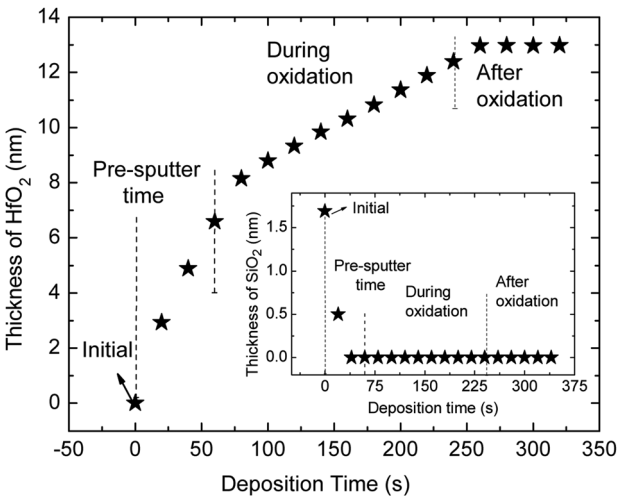

FIG. 5. Thickness profile of HfO_2 layer is shown with respect to the deposition time of the film measured simultaneously during and after the film growth process, while inset plot shows the thickness profile of interfacial SiO_2 layer as a function of deposition time during and after film growth process.

first measurement of SiO_2 thickness was undertaken immediately after fixing the substrate on the substrate holder of the deposition system and was measured to be 1.62 nm which was found to decrease rapidly during the deposition of Hf metal. It is observed from Fig. 5 that thickness of SiO_2 reduces to zero even before completion of Hf metal deposition and continues to remain zero even after completion of HfO_2 deposition process. The *in-situ* SE study clearly demonstrates the absence of SiO_2 and/or SiO_x suboxide interfacial layer for the films reported in the present paper.

Only after Hf metal buffer layer deposition, oxygen gas was introduced into the chamber for the deposition of HfO_2 film. However, even before deposition of HfO_2 film, HfO_2 thickness measurement was started during the deposition of Hf metal buffer layer (at 20 s) and was continued with time intervals of 20 s till the completion of the deposition of HfO_2 thin film. It can be seen from Fig. 5 that thickness of HfO_2 increases with the increment in deposition time. The deposition rate was measured to be 3.63 nm/min during Hf metal buffer layer deposition and decreases to 2.11 nm/min during HfO_2 film deposition. During Hf metal deposition process, highly reactive sputtered Hf atoms are produced due to argon bombardment, which consume some of the oxygen of SiO_2 to produce HfO_2 films. It is well known[26,41] that oxygen radicals oxidize the Hf metal more selectively than silicon substrate which, in turn, results in the observed decrease in SiO_2 thickness as shown in the inset of Fig. 5. It is also known that the deposition rate is influenced by the energy as well as the rate of impinging particles. When oxygen gas along with argon is introduced to the deposition chamber for the purpose of HfO_2 film formation, energy is required both for the molecular motion and the dissociation of O_2 molecules which is taken from the discharge plasma. This energy loss leads to a reduction in the ionization process[42] which results in the decrease in the deposition rate to 2.11 nm/min with the introduction of oxygen gas into the deposition chamber.

The transmission coefficient, T, reflection coefficient, R, corresponding to the final stage of HfO_2 film as a function of wavelength are shown in Figs. 6(a) and 6(b), respectively. The variation of transmission coefficient with wavelength clearly reveals that HfO_2 film is transparent to the light of wavelength greater than 400 nm, thus justifying to the Cauchy model usage for the studied films. The variation of refractive index, n, of the film with wavelength is displayed in Fig. 7. Since the value of n at the wavelength of 632.8 nm is found to be 2.01 which is very close to the value of bulk HfO_2 ($n = 2.11$),[43] this implies that the grown HfO_2 film has a compact structure.

B. FTIR study

The bonding configurations of the grown film studied by FTIR spectra are shown in Fig. 8. The FTIR measurement has been taken in 400–1200 cm^{-1} range since the lower wavenumber region (<1300 cm^{-1}) contains the significant modes of HfO_2 and SiO_2. The peak located near 670 cm^{-1} is related to C-O mode present in the background. The band near 610 cm^{-1} has been assigned to the absorbance of strong Si phonon[44,45] which is of no interest to the present study.

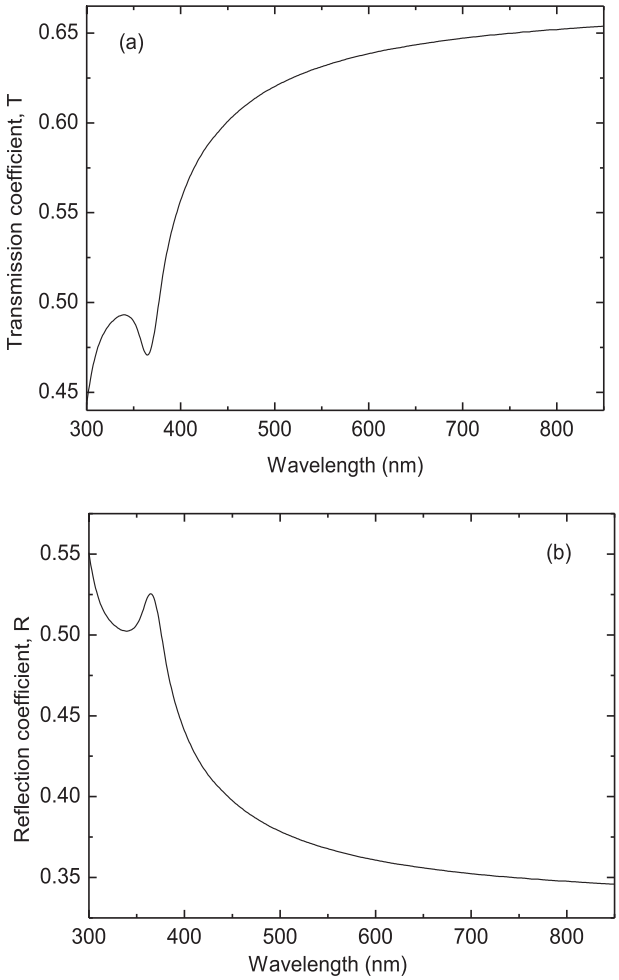

FIG. 6. For the grown HfO_2 film (a) transmission coefficient vs wavelength and (b) reflection coefficient vs wavelength.

Several modes associated with HfO_2 are observed near 420, 513, and 735 cm^{-1}. The position of these modes is in agreement with that of the monoclinic HfO_2 crystals.[45,46] Basa *et al*. have reported that the SiO_2 stretch modes are peaked near 1070 cm^{-1}, while the suboxide SiO_x ($x < 2$)

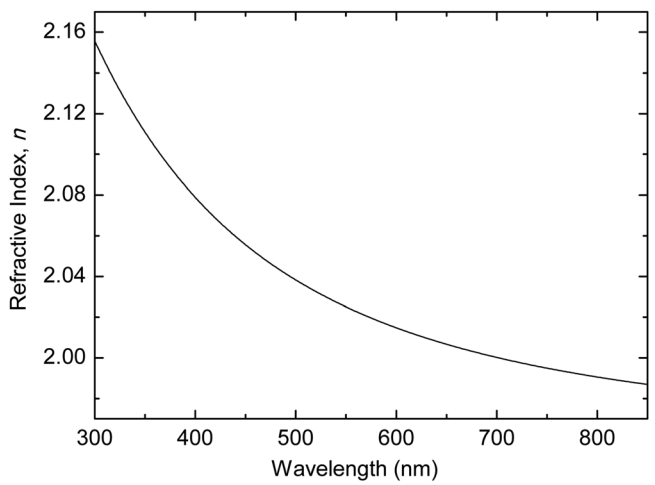

FIG. 7. Refractive index versus wavelength is given for the surface layer of grown film. Note that the refractive index of bulk HfO_2 is 2.11 at 632 nm wavelength.

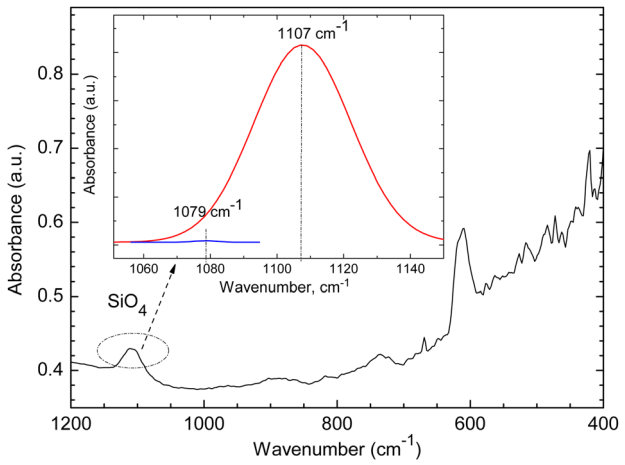

FIG. 8. Absorbance spectra of the grown film obtained from FTIR measurement. The deconvolution of the peak from 1050 to 1150 cm^{-1} is shown in the inset.

stretch modes are located in the region from about 989 to 1057 cm^{-1}.[47] It is obvious from Fig. 8 that the region from 989 to 1057 cm^{-1} does not contain any peaks corresponding to SiO_x suboxide. Moreover, the observed peak was deconvoluted in the region from 1050 to 1150 cm^{-1} by fitting with the Gaussian curves pertaining to SiO_2 and SiO_x peaks.

The best fit of the observed peak, shown in the inset of Fig. 8, was obtained with two peaks centered near 1107 cm^{-1} and 1079 cm^{-1} with "*r*-square" as 0.9987 and "reduced chi square" as 2.42×10^{-7}. The closer the fit is to the data points, the closer will be the value of "r-square" and "reduced chi square" to 1 and 0, respectively. Therefore, our obtained fit result is extremely good. The vanishingly small intensity of the peak near 1079 cm^{-1} which corresponds to Si-O-Hf bonds seems to indicate the almost near absence of these in the interfacial region of the studied films since this peak is due to the formation of $HfSi_xO_y$ interface.[45] The clear absence of peak near 1070 cm^{-1} and/or below has established conclusively that SiO_2 and/or SiO_x stretch modes are absent in the studied films but has revealed the presence of the peak near 1107 cm^{-1} due to SiO_4.[45] These results are in agreement with the *in-situ* SE analysis.

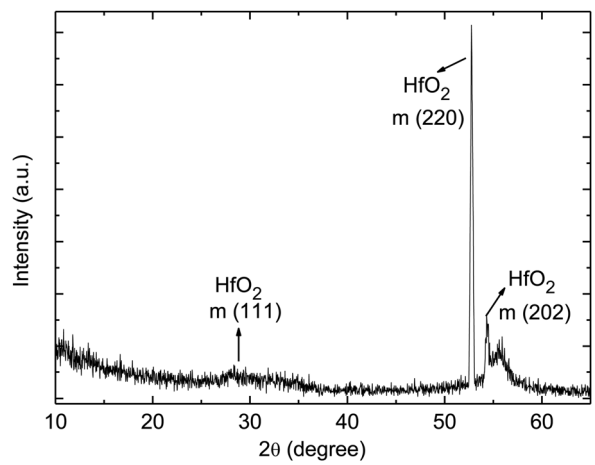

FIG. 9. XRD spectra of the grown film, measured with grazing incidence mode with an incidence angle of 0.5°.

C. XRD study

Figure 9 displays XRD spectra of the grown film. The film has a very low intensity peak at 2θ of 28° corresponding to $\langle 111 \rangle$ reflection plane of monoclinic structure of HfO_2.[48] The observed peaks near 52.7° and 54.4° have reasonable intensity and are attributed to $\langle 220 \rangle$[49] and $\langle 202 \rangle$[48,50] reflection planes of monoclinic HfO_2 structure. The monoclinic structure as revealed by XRD is also in agreement with our FTIR results. Formation of crystalline phase even for the room temperature deposited HfO_2 films may be attributed to the very low crystallization temperature of amorphous HfO_2 films[45] as well as to the possible reduction of the crystallization temperature due to metal induced crystallization.

V. CONCLUSIONS

Reactive rf magnetron sputtering system along with the attached *in-situ* spectroscopic ellipsometer was used to grow and characterize high-κ HfO_2 films deposited on *n*-type $\langle 100 \rangle$ crystalline silicon substrate. Before HfO_2 film growth was realized, Hf metal buffer layer was deposited on Si substrate in order to study the possible elimination of unwanted interfacial layer formation, if any, between HfO_2 film and silicon substrate. The grown films were characterized by FTIR and GIXRD in addition to spectroscopic ellipsometric analysis. The important conclusions of this study are

(i) The depth profile was probed optically by *in-situ* SE measurements at defined time intervals. It reveals that Hf metal buffer layer has consumed some oxygen of natural SiO_2 and has resulted in the formation of HfO_2 layer even before starting of the reactive oxidation by involving O_2, necessary for the formation of HfO_2 film. Furthermore, *in-situ* SE measurements have also demonstrated the prevention of SiO_2 formation and/or suboxide SiO_x interfacial layer, which is found to be in agreement with our FTIR results. Thus, the predeposited Hf metal buffer layer is shown to play an important role in eliminating the formation of unwanted interfacial layer.

(ii) The monoclinic crystal structure, also consistent with FTIR results, is established for the studied HfO_2 films by GIXRD in spite of the film deposition being carried out at room temperature.

ACKNOWLEDGMENTS

This research was supported mainly by The Scientific and Technological Research Council of Turkey (TUBITAK) with Project Nos. 107T117, 113F349, and partially by Izmir Institute of Technology with research Project No. 2008 IYTE 37. We would like to thank "Applied Quantum Research Center (UKAM)" located at the Physics Department of IZTECH.

[1]K. Kobashi, T. Nagata, A. Ogura, T. Nabatame, and T. Chikyow, J. Appl. Phys. **114**, 014106 (2013).
[2]A. Cantas, G. Aygun, and R. Turan, "Impact of incorporated oxygen quantity on optical, structural and dielectric properties of reactive magnetron sputter grown high-k HfO_2/Hf/Si thin film," Appl. Surf. Sci. (in press).
[3]G. D. Wilk, R. M. Wallace, and J. M. Anthony, J. Appl. Phys. **89**, 5243 (2001).
[4]*High Dielectric Constant Materials: VLSI MOSFET Applications*, edited by M. Houssa (IOP, London, 2003).
[5]G. Aygun and R. Turan, Thin Solid Films **517**, 994 (2008).
[6]J. Yota, J. Electrochem. Soc. **156**(11), G173 (2009).
[7]K. F. Albertin and I. Pereyra, Microelectron. Eng. **77**, 144 (2005).
[8]G. Aygun, E. Atanassova, A. Alacakir, L. Ozyuzer, and R. Turan, J. Phys. D: Appl. Phys. **37**, 1569 (2004).
[9]J. Robertson, Rep. Prog. Phys. **69**, 327 (2006).
[10]H. J. Hubbard and D. G. Schlom, J. Mater. Res. **11**, 2757 (1996).
[11]D. G. Schlom and J. H. Haeni, MRS Bull. **27**, 198 (2002).
[12]G. Aygun, A. Cantas, Y. Simsek, and R. Turan, Thin Solid Films **519**, 5820 (2011).
[13]M. Gutowsky, J. E. Jaffe, C. L. Liu, M. Stoker, R. I. Hegde, R. S. Rai, and P. J. Tobin, Appl. Phys. Lett. **80**, 1897 (2002).
[14]J. Kwo, M. Hong, A. R. Kortan, K. T. Queeney, Y. J. Chabal, J. P. Mannaerts, T. Boone, J. J. Krajewski, A. M. Sergent, and J. M. Rosamilia, Appl. Phys. Lett. **77**, 130 (2000).
[15]Y. H. Wu, M. Y. Yang, A. Chin, W. J. Chen, and C. M. Kwei, IEEE Electron Device Lett. **21**, 341 (2000).
[16]M. Copel, M. Gribelyuk, and E. Gusev, Appl. Phys. Lett. **76**, 436 (2000).
[17]M. Dong, H. Wang, L. Shen, Y. Ye, C. Ye, Y. Wang, J. Zhang, and Y. Jiang, J. Mater. Sci.: Mater. Electron. **23**, 174 (2012).
[18]M. A. Sahiner, P. S. Lysaght, J. C. Woicik, C. S. Park, J. Huang, G. Bersuker, W. Taylor, P. D. Kirsch, and R. Jammy, Phys. Status Solidi A **209**, 679 (2012).
[19]Q. Fang, J.-Y. Zhang, Z. Wang, M. Modreanu, B. J. O'Sullivan, P. K. Hurley, T. L. Leedham, D. Hywel, M. A. Audier, C. Jimenez, J.-P. Senateur, and I. W. Boyd, Thin Solid Films **453–454**, 203 (2004).
[20]V. Pervak, F. Krausz, and A. Apolonski, Thin Solid Films **515**, 7984 (2007).
[21]T. J. Bright, J. I. Watjen, Z. M. Zhang, C. Muratore, and A. A. Voevodin, Thin Solid Films **520**, 6793 (2012).
[22]P. D. Kirsch, C. S. Kang, J. Lozano, J. C. Lee, and J. G. Ekerdt, J. Appl. Phys. **91**, 4353 (2002).
[23]S. Hayashi, K. Yamamoto, Y. Harada, R. Mitsuhashi, K. Eriguchi, M. Kubota, and M. Niwa, Appl. Surf. Sci. **216**, 228 (2003).
[24]R. Tan, Y. Azuma, and I. Kojima, Appl. Surf. Sci. **222**, 346 (2004).
[25]D. A. Glocker and S. Ismat, *Hand Book of Thin Film Process Technology* (IOP publishing, Bristol and Philadelphia, 1999).
[26]G. Aygun and I. Yildiz, J. Appl. Phys. **106**, 014312 (2009).
[27]D. K. Basa, G. Abbate, G. Ambrosone, U. Coscia, and A. Marino, J. Appl. Phys. **107**, 023502 (2010).
[28]H. Fujiwara, *Spectroscopic Ellipsometry: Principles and Applications* (John Wiley and Sons, England, 2007).
[29]H. G. Tompkins and E. A. Irena, *Handbook of Ellipsometry* (William Andrew Publishing, 2005).
[30]O. Buiu, W. Davey, Y. Lu, I. Mitrovic, and S. Hall, Thin Solid Films **517**, 453 (2008).
[31]M. M. A. G. Jafar, Eur. Int. J. Sci. Technol. **2**, 214 (2013), available at http://www.eijst.org.uk/images/frontImages/gallery/Vol._2_No._5_/20.pdf.
[32]D. J. Griffiths, *Introduction to Electrodynamics* (Prentice-Hall, 1999), p. 386.
[33]U. Richter, *Modelling, Simulation and Fits for Enhancing Discrete wavelength Ellipsometers* (Sentech Simulation Software Manual, 1995), p. 17.
[34]W. Rzodkiewicz and A. Panas, Acta. Phys. Pol. A **116**, 92 (2009), available at http://przyrbwn.icm.edu.pl/APP/PDF/116/a116zs24.pdf.
[35]H. Xie, F. L. Ng, and X. T. Zeng, Thin Solid Films **517**, 5066 (2009).
[36]H. G. Tompkins, *A User's Guide to Ellipsometry* (Academic Press, London, 1993), p. 28.
[37]J. M. Khoshman and M. E. Kordesch, Surf. Coat. Technol. **201**, 3530 (2006).
[38]C. M. Herzinger, B. Johs, W. A. McGahan, J. A. Woollam, and W. Paulson, J. Appl. Phys. **83**, 3323 (1998).
[39]G. Aygun, E. Atanassova, R. Turan, and Tz. Babeva, Mater. Chem. Phys. **89**, 316 (2005).
[40]G. He, L. D. Zhang, G. H. Li, M. Liu, L. Q. Zhu, S. S. Pan, and Q. Fang, Appl. Phys. Lett. **86**, 232901 (2005).
[41]K. Yamamoto, S. Hayashi, M. Niwa, M. Asai, S. Horii, and H. Miya, Appl. Phys. Lett. **83**, 2229 (2003).
[42]S. Duenas, H. Castan, H. Garcia, A. Gomez, L. Bailon, M. Toledano-Luque, I. Martil, and G. Gonzalez-Diaz, Semicond. Sci. Technol. **22**, 1344 (2007).
[43]G. He, L. Q. Zhu, M. Liu, Q. Fang, and L. D. Zhang, Appl. Surf. Sci. **253**, 3413 (2007).

[44]M. M. Frank, S. Soyan, S. Dormann, T. J. Emge, L. S. Wielunski, E. Garfunkel, and Y. J. Chabal, Mater. Sci. Eng., B **109**, 6 (2004).
[45]D. A. Neumayer and E. Cartier, J. Appl. Phys. **90**, 1801 (2001).
[46]M. T. Luque, E. san Andres, A. del Prado, I. Martil, M. L. Lucia, G. G. Diaz, F. L. Martinez, W. Bohne, J. Rohrich, and E. Strub, J. Appl. Phys. **102**, 044106 (2007).
[47]D. K. Basa and F. W. Smith, Thin Solid Films **192**, 121 (1990).
[48]R. E. Hann, P. R. Suitch, and J. L. Pentecost, J. Am. Ceram. Soc. **68**, C-285 (1985).
[49]L. P. Feng, Z. T. Liu, and Y. M. Shen, Vacuum **83**, 902 (2009).
[50]G. He, M. Liu, L. Q. Zhu, M. Chang, Q. Fang, and L. D. Zhang, Surf. Sci. **576**, 67 (2005).